Research Article

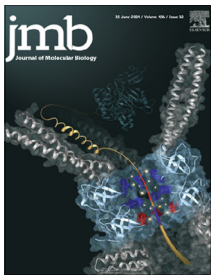

# AIDA-1/ANKS1B Binds to the SynGAP Family RasGAPs with High Affinity and Specificity

**Xueqian Wang** [1,†,*], **Yu Wang** [2,5,†], **Qixu Cai** [3] **and Mingjie Zhang** [4,5,*]

*1 - **Biomedical Research Institute,** Shenzhen Peking University-The Hong Kong University of Science and Technology Medical Center, Shenzhen 518036, China*
*2 - **Division of Life Science,** Hong Kong University of Science and Technology, Clear Water Bay, Kowloon, Hong Kong, China*
*3 - **State Key Laboratory of Vaccines for Infectious Diseases,** School of Public Health, Xiamen University, Xiamen, Fujian, China*
*4 - **Greater Bay Biomedical Innocenter,** Shenzhen Bay Laboratory, Shenzhen 518036, China*
*5 - **School of Life Sciences,** Southern University of Science and Technology, Shenzhen 518055, China*

***Correspondence to Xueqian Wang and Mingjie Zhang:** xueqwang@pku.edu.cn (X. Wang), zhangmj@sustech.edu.cn (M. Zhang)*
https://doi.org/10.1016/j.jmb.2024.168608
***Edited by Zhi-Jie Liu***

## Abstract

AIDA-1, encoded by *ANKS1B*, is an abundant postsynaptic scaffold protein essential for brain development. Mutations of *ANKS1B* are closely associated with various psychiatric disorders. However, very little is known regarding the molecular mechanisms underlying AIDA-1′s involvements under physiological and pathophysiological conditions. Here, we discovered an interaction between AIDA-1 and the SynGAP family Ras-GTPase activating protein (GAP) via affinity purification using AIDA-1d as the bait. Biochemical studies showed that the PTB domain of AIDA-1 binds to an extended NPx[F/Y]-motif of the SynGAP family proteins with high affinities. The high-resolution crystal structure of AIDA-1 PTB domain in complex with the SynGAP NPxF-motif revealed the molecular mechanism governing the specific interaction between AIDA-1 and SynGAP. Our study not only explains why patients with *ANKS1B* or *SYNGAP1* mutations share overlapping clinical phenotypes, but also allows identification of new AIDA-1 binding targets such as Ras and Rab interactors.


## Introduction

The AIDA-1 (abbreviated from Amyloid-Beta Protein Precursor Intracellular Domain Associated Protein 1) multi-domain scaffold proteins, encoded by *ANKS1B*, are expressed exclusively in brain tissue, including the cerebral cortex, striatum, hippocampus, and other regions.[1,2] Human genetic studies have linked AIDA-1 to various neuropsychiatric disorders such as autism spectrum disorder (ASD),[1,3,4] schizophrenia,[5,6] mood disorder,[7,8] and obsessive compulsive disorder.[9,10] AIDA-1 is highly abundant and specifically enriched at postsynaptic densities (PSD).[1,11] Quantitative proteomic studies indicated that the amount of AIDA-1 in PSD is at ~50% of PSD-95, which is one of the most abundant and important protein in the PSD.[12] However, very little is known regarding the molecular mechanisms underlying AIDA-1′s function in neuronal synapses, at least partly due to our poor knowledge on molecular interactions involving AIDA-1.

When a synapse is stimulated, AIDA-1 was observed to move from the core to the peripheral regions of the PSD, a phenomenon that is analogous to the activity-induced dispersion of SynGAP from PSD core.[13–17] SynGAP is another highly abundant PSD protein that is known to bind PSD-95 like AIDA-1 via their C-terminal PDZ bind-

ing motif (PBM).[18,19] Interestingly, patients with mutations in *ANKS1B* or *SynGAP1* share overlapping clinical phenotypes.[1,20,21] Mice with removal of one allele of *ANKS1B* or *SynGAP1* also show similar ASD-like phenotypes.[1,20] In *SynGAP1*$^{+/-}$ mice, AIDA-1 was correspondingly reduced.[21] These reported studies suggest that AIDA-1 and SynGAP may function together in synapses in orchestrating brain functions, though direct evidence supporting this hypothesis is lacking. The fact that loss of one allele of *ANKS1B* in humans as well as in rodents can cause brain function defects indicates the importance of the absolute concentration of AIDA-1 in neuronal functions.

Alternative splicing of *ANKS1B* generates long and short forms of AIDA-1 (Figure 1A). All isoforms of AIDA-1 share a pair of sterile alpha motif (SAM) domains connected in tandem, a phosphotyrosine binding (PTB) domain, and a very C-terminal tail PBM (Figure 1A). The long isoforms of AIDA-1 (e.g., AIDA-1b) contain an additional N-terminal fragment of ~800 amino acid residues with an ankyrin repeat sequence at the very N-terminal end (Figure 1A). AIDA-1b, AIDA-1c, and AIDA-1d are the main variants enriched in synapses and in the PSD.[1] During development, the expression levels of the three AIDA-1 variants vary in the mouse brain, with AIDA-1b being the predominant variant in the embryonic stage and AIDA-1c and AIDA-1d expressed after birth and in the mature brains.[2] The multi-domain feature of AIDA-1 suggests that AIDA-1 may function as a scaffold capable of binding to different target proteins in neuronal synapses. The structures of the SAM1-SAM2 tandem and the apo-form of the PTB domain have been determined.[22,23] Other than a reported weak interaction (Kd ~ 10 μM) between the PTB domain of AIDA-1 and the NPxY-motif of amyloid precursor protein (APP),[23,24] no binding targets are known for the ankyrin repeats, the SAM domains, and the PTB domain of AIDA-1. Accordingly, it is not known why mutations of *ANKS1B* can cause brain disorders.

We discovered in this study that the SynGAP family RasGAPs (SynGAP, Dab2IP, and RASAL2) specifically and strongly bind to the PTB domain of AIDA-1. The crystal structure of AIDA-1 PTB in complex with its binding NPxF-motif from SynGAP elucidates the molecular basis underlying the specific interaction between these two abundant and functionally connected PSD proteins. The interaction mode revealed by the complex structure also allows identification of other previously unknown AIDA-1 binding target proteins such as Ras and Rab interactors. Given that *SynGAP1* is one of the highest ranked genes associated with neurodevelopmental disorders[20,25–28] and with autisms and that AIDA-1 is among very few specific SynGAP binding proteins known to date, the results presented in this study will be valuable for understanding roles of AIDA1 and SynGAP in brain functions and for correcting brain function defects caused by mutations of *ANKS1B* and *SynGAP1*.

## Results

### The PTB domain of AIDA-1 binds to SynGAP with a high affinity

To explore the role of AIDA-1 in the brain and its association with neurodevelopmental disorders, we attempted to identify AIDA-1 binding proteins in the mouse brain by affinity purification coupled with mass spectrometry (Figure S1A). Since the short isoforms of AIDA-1 (AIDA-1c/1d) are the predominantly expressed isoforms in the mature mouse brain, we used AIDA-1d (residues 36–506) as the affinity purification bait. We removed the C-terminal PBM as we intentionally wanted to avoid purifying PDZ domain proteins in our purification due to the fact that AIDA-1 is known to bind to PSD-95 PDZ domains via its PBM. The N-terminal 35 residues were removed to improve the bait protein quality. SynGAP, Dab2IP, and RASAL2 were identified as top ranked AIDA-1d associating proteins, with the peptide sequence coverage ranging from 73% to 89% (Figure 1B). All three proteins are RasGAP proteins and share a similar domain organization (Figure 1C). Upon further analysis of the sequences of SynGAP, Dab2IP, and RASAL2, we found that they all share a NPx[F/Y] sequence motif (N, Asn; P, Pro; x, any amino acid; F, Phe; Y, Tyr) known to bind to PTB domains (Figures 1C and S1B).[29–32] This NPx[F/Y]-motif and five residues preceding the motif are

**Figure 1. AIDA-1 PTB binds to the SynGAP with a high affinity.** (A) Schematic diagram showing the domain organization of AIDA-1. (B) The recovered peptides and coverages of the protein sequences of the affinity purified AIDA-1 binding proteins by mass spectrometry. (C) Domain organizations of the AIDA-1 binding SynGAP family RasGAPs. (D) Sequence alignment of the NPx[Y/F] motif of SynGAP from different species. (E) The binding of SynGAP-NPxF (amino acids 924–934) to AIDA-1d-ΔN (amino acids 36–510) measured by ITC. SynGAP-NPxF (500 μM) in the syringe was titrated into AIDA-1d-ΔN (50 μM) in the cell. (F) SEC-MALS assay showing the stable and 1:1 stoichiometric complex formation between AIDA-1d-ΔN and SynGAP-NPxF. The fitted molecular weights are expressed as the best fitted values ± SE. (G) Summary of ITC-based measurements of the binding affinities between variant fragments of AIDA-1 and SynGAP. (H) The binding of SynGAP-NPxF to AIDA-1 PTB (AIDA-1c aa203–360) measured by ITC. SynGAP-NPxF (500 μM) in the syringe was titrated into AIDA-1-PTB (50 μM) in the cell.

A

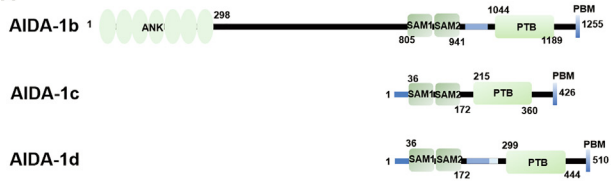


B

| Protein | Peptides | Coverage (%) |
|---|---|---|
| SynGAP | 262 | 89 |
| Dab2IP | 187 | 88 |
| RASAL2 | 91 | 73 |

C

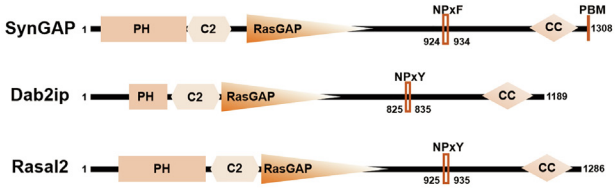


D

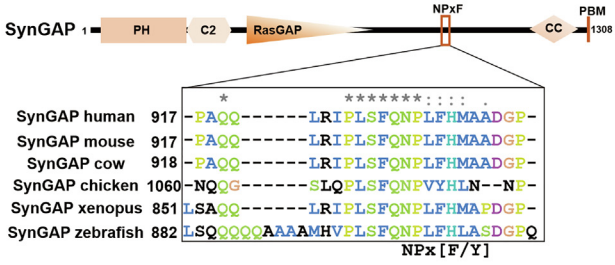


E

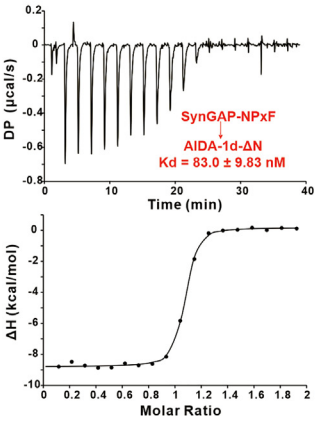


F

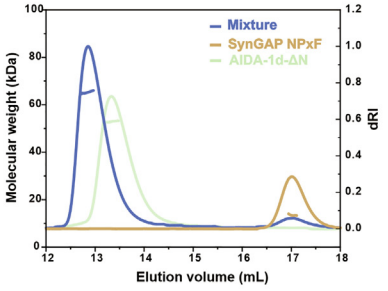


| MW (kDa) | Theoretical | Fitted |
|---|---|---|
| AIDA-1d-ΔN | 53.9 | 52.9 ± 1.1 |
| Trx SynGAP NPxF motif | 15.8 | 13.4 ± 0.5 |
| 1:1 complex | 69.7 | 65.3 ± 0.9 |

G

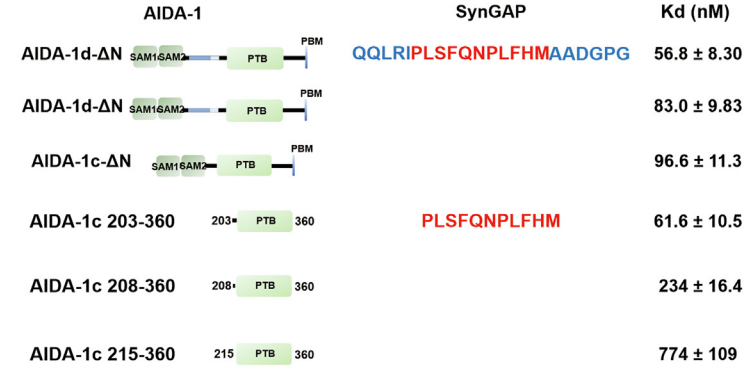


H

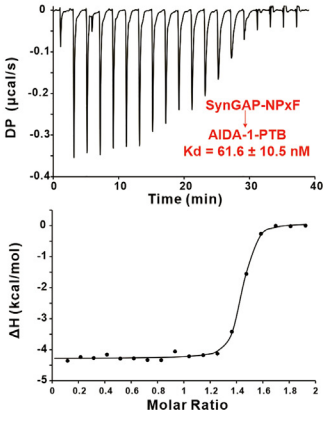

highly conserved in SynGAP from vertebrates (Figure 1D). Thus, we hypothesized that AIDA-1 might directly bind to the NPxF-motif of SynGAP via its PTB domain.

To test this hypothesis, we assayed the binding between the near full-length AIDA-1d (residues 36–510, termed "AIDA-1d-ΔN") and a 11-residue fragment of SynGAP containing the NPxF-motif (PLSFQNPLFHM, residues 924–934, termed "SynGAP-NPxF") using isothermal titration calorimetry (ITC) experiment. The ITC experiment showed that AIDA-1d-ΔN binds to SynGAP-NPxF with a Kd ∼ 83 nM (Figure 1E), which is more than 100-fold higher than the previously reported binding between AIDA-1 PTB and APP NPxY-motif.[23] The size exclusion chromatography coupled with multi-angle light scattering (SEC-MALS) experiment further confirmed that AIDA-1d-ΔN and SynGAP-NPxF formed a stable 1:1 stoichiometric complex (Figure 1F). Elongating the SynGAP-NPxF motif by 5 residues at both ends (QQLRIPLSFQNPLFHMAADGPG, residues 919–940) only slightly enhanced the peptide's binding to AIDA-1d, indicating that the 11-residue SynGAP-NPxF motif is chiefly responsible for SynGAP to bind to AIDA-1d (Figures 1G and S1C). We further showed that AIDA-1c also binds to SynGAP-NPxF with an affinity comparable to that of AIDA-1d (Figure 1G).

We then mapped the minimal SynGAP binding sequence of AIDA-1 by ITC (Figures 1G, 1H, S1E and S1F). The data showed that neither the SAM1 and SAM2 domain nor the PBM of AIDA-1 is involved in binding. Further mapping revealed that the canonical PTB domain with a short N-terminal extension (i.e., residues 203–360 based on the AIDA-1c sequence and termed "AIDA-1-PTB") is sufficient in binding to SynGAP-NPxF (Figures 1H and S1C). Since the region corresponding to residues 203–360 of AIDA-1c are shared among all isoforms of the AIDA-1 family protein, we expect that all isoforms of AIDA-1 can bind to SynGAP. The boundary of the PTB domain of AIDA-1c used to solve its structure by NMR Spectroscopy (PDB: 2 M38, residues 219–353 in AIDA-1c)[23] is shorter than the one characterized in the current study. We demonstrated that truncating the PTB domain from residue 203 progressively weakened its binding to SynGAP-NPxF (Figures 1G and S1E).

We further verified the interaction between AIDA-1 and the NPxY motifs of the other two SynGAP family RasGAP proteins, Dab2IP and RASAL2, by ITC assays (Figure S2). The results showed that Dab2IP and RASAL2, via their respective NPxY motifs, bind to AIDA-1c/1d PTB with a Kd ∼ 70 nM. Taken together, the above biochemistry experiments demonstrate that AIDA-1 can specifically bind to all three members of the SynGAP family RasGAPs existing in the mice brain.

## The structure of the AIDA-1-PTB/SynGAP-NPxF complex

To understand the detailed molecular mechanism governing the strong interaction between AIDA-1 and SynGAP, we solved the crystal structure of AIDA-1-PTB in complex with SynGAP-NPxF to the resolution of 2.00 Å (Figures 2; Table 1). Electron densities for nearly all residues of the two molecules in the complex are clearly defined (Figure S3A). The NPxF-motif of SynGAP is characterized by a Phe residue (Phe932 and referred to as residue 0) and the residues preceding Phe(0) are numbered from −8 to −1 (Figures 2B and 2C).

The AIDA-1-PTB domain in the complex contains a canonical PTB fold plus an N-terminal extension corresponding to residues 205–224 containing the α0-helix (Figures 2A and S3B). SynGAP-NPxF binds to an elongated, highly hydrophobic groove between α2 and β5 of the AIDA-1 PTB domain via forming antiparallel β-sheet with β5, a binding mode typical for the interactions of PTB domains with target peptides.[29,30,32]

The interaction interface between AIDA-1 PTB domain and SynGAP-NPxF can be divided into three regions: region 1 between the N-terminal extension of AIDA-1 PTB domain and SynGAP-NPxF, region 2 between the residues located outside the canonical NPx[F/Y] motif (i.e., residues−8, −7, −6, −5, and −4) of the SynGAP NPxF-motif and AIDA-1-PTB, and region 3 between AIDA-1-PTB and the core of NPxF-motif (Figure 3A).

As shown in Figure 3B, the N-terminal extension of AIDA-1 PTB actively engages in binding to SynGAP. The backbone carbonyl of Ala207 from PTB forms a hydrogen bond with the side chain of Gln(−4) of SynGAP-NPxF. The hydrophobic side chains P210 and Y212 interact with hydrophobic residues from the α2 helix (L342 and Y352) forming part of the target peptide binding hydrophobic groove, explaining why residues before the canonical β1 strand of the canonical PTB are important for AIDA-1 to bind to SynGAP.

The interactions in region 2 are very specific in the AIDA-1-PTB/SynGAP-NPxF complex. Every residue preceding the NPxF sequence of SynGAP (i.e., from residue −8 to −4) is intimately involved in binding to PTB mainly via hydrophobic interactions and supplemented by hydrogen bonds (Figures 2B, C and 3C). Thus, residues from −8 to −4 are critical for the strong binding of SynGAP-NPxF to AIDA-1. It is noted that the residues from positions −8 to −4 are completely conserved in vertebrate SynGAP (Figure 1D) and among the three SynGAP family RasGAPs (Figure S1B), further supporting the critical roles of these residues for the SynGAP/AIDA-1 interaction.

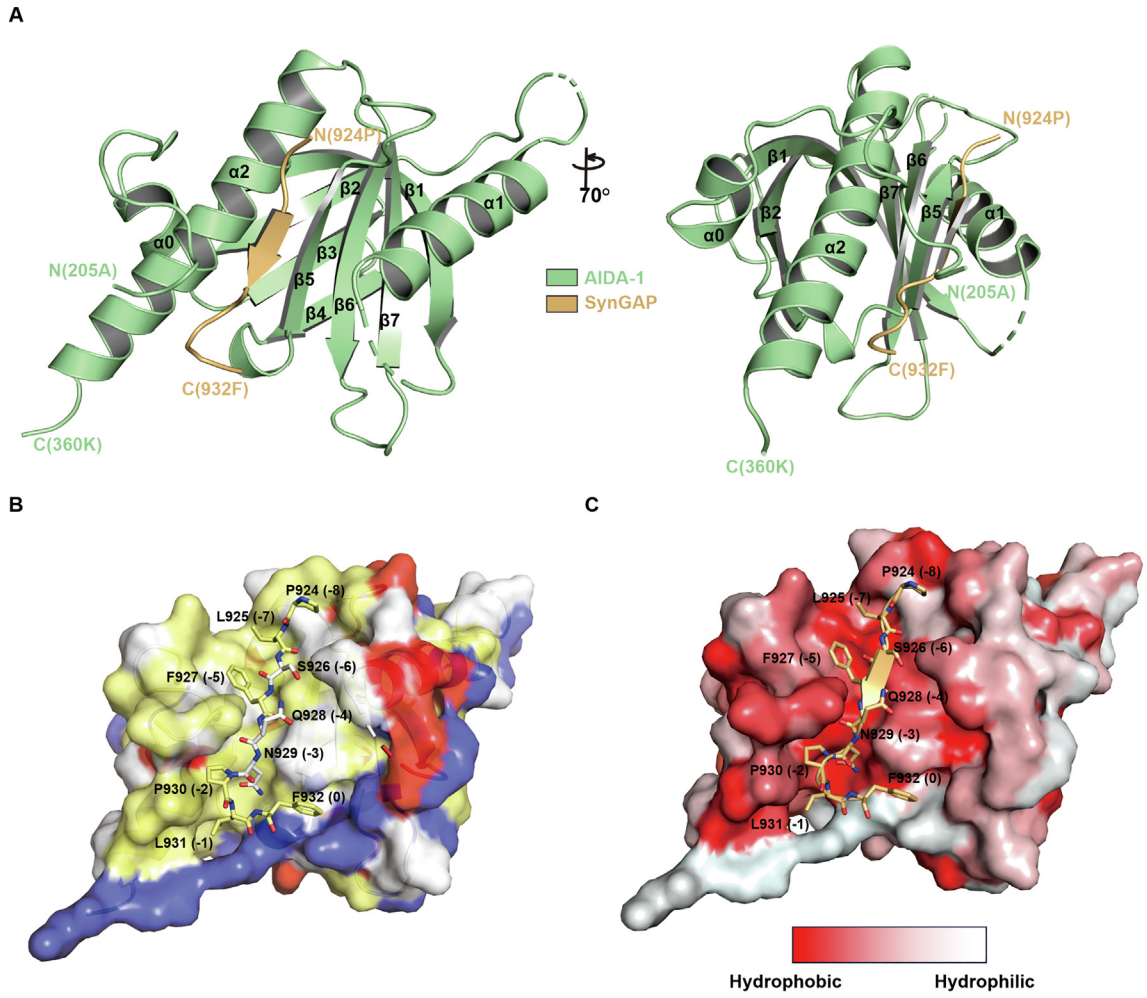


**Figure 2. Crystal Structure of AIDA-1-PTB in Complex with SynGAP-NPxF.** (A) Ribbon diagram representation of the overall structure of AIDA-1-PTB in complex with SynGAP-NPxF. The SynGAP-NPxF is colored yellow. The AIDA-1-PTB is colored pale green. The scheme is used throughout the paper. (B) The combined surface (AIDA-1-PTB) and stick (SynGAP-NPxF) models showing the interaction between AIDA-1-PTB and SynGAP-NPxF. In the surface model, the positively charged amino acids of AIDA-1 are highlighted in blue, the negatively charged residues in red, the hydrophobic residues in yellow, the polar uncharged residue and Gly in white. (C) The hydrophobic surface (AIDA-1-PTB) and stick (SynGAP-NPxF) model showing the hydrophobic interaction between AIDA-1-PTB and SynGAP-NPxF. In the hydrophobic surface of model, the intensity of redness is indicative of the hydrophobicity level.

The interaction in region 3 involves the NPxF sequence of SynGAP with the PTB, and this interaction is the same as other well-characterized NPx[F/Y]-motif/PTB interactions in the literature and we will not go into details here (Figures 3D, S4A and S4B).[29,31–33]

We next validated the roles of some of the interactions observed in the structure of the complex between SynGAP NPxF-motif and the PTB domain of AIDA-1 using a mutagenesis approach combined with quantitative ITC-based binding assays (Figures 3E–3L, S4C and S4D). Substitutions of the hydrophobic residues of the SynGAP NPxF-motif (L925 at position −7, F927 at position −5, and F932 at position 0) with Ala individually dramatically weakened or nearly abolished the AIDA-1-PTB/SynGAP binding. The results of ITC (Figure 3H) show that substitution of F927(−5) by Arg completely abolished the binding between AIDA-1 and SynGAP. The critical residue Asn(−3) of the SynGAP NPxF motif was replaced with Ala, and the substitution disrupted SynGAP's binding to AIDA-1 as shown in Figure S4C. Expectedly, replacing Phe(−5) in the NPxY motifs of Dab2IP and RASAL2 with a polar Arg also abolished the binding of Dab2IP or RASAL2 to AIDA-1 (Figures S4E and S4F). Correspondingly, substituting L342 in AIDA-1 PTB (L342 is in α1 of PTB and is involved in binding to the NPxF motif as well as stabilizing the α0 helix; see Figure 3C) with Glu reduced the PTB domain's binding to the SynGAP NPxF motif by ~70-fold (Figure 3K);

Table 1 X-ray data collection and refinement statistics.

| Data collection | SynGAP/AIDA-1 |
|---|---|
| Space group | I23 |
| Wavelength (Å) | 0.97852 |
| Unit cell parameters a, b, c (Å) | 112.919 |
| α, β, γ (°) | 90 |
| Resolution range (Å) | 50–2.00 (2.03–2.00) |
| No. of unique reflections | 16,295 (808) |
| Redundancy | 39.0 (40.6) |
| I/σ | 35.6 (1.5) |
| Completeness (%) | 100.0 (100.0) |
| $R_{merge}$ [a] (%) | 17.6 (251.7) |
| $CC_{1/2}$ | 0.995 (0.697) |
| Structure refinement | |
| Resolution (Å) | 2.00 |
| $R_{work}$ [b] (%) | 21.31 |
| $R_{free}$ [c] (%) | 26.38 |
| RMSD bonds (Å) | 0.007 |
| RMSD angles (°) | 1.365 |
| Average B factor (Å$^2$) | 54.8 |
| No. of atoms | |
| Protein | 1255 |
| Ligand/ion | 0 |
| Water | 30 |
| B factors (Å$^2$) | |
| Proteins | 57.9 |
| Ligand/ion | 0 |
| Water | 57.4 |
| Ramachandran plot | (%) |
| Preferred | 92.52 |
| Allowed | 7.48 |
| Outliers | 0 |

Numbers in parentheses represent the values for the highest-resolution shell.

[a] $R_{merge} = \Sigma|I_i - <I>|/\Sigma I_i$, where $I_i$ is the intensity of measured reflection and $< I >$ is the mean intensity of all symmetry-related reflections.

[b] $R_{work} = \Sigma_W||F_{calc}| - |F_{obs}||/\Sigma|F_{obs}|$, where $F_{obs}$ and $F_{calc}$ are observed and calculated structure factors. W is working dataset of about 95% of the total unique reflections randomly chosen and used for refinement.

[c] $R_{free} = \Sigma_T||F_{calc}| - |F_{obs}||/\Sigma|F_{obs}|$, where T is a test dataset of about 5% of the total unique reflections randomly chosen and set aside prior to refinement.

substitution of F348 in PTB (F348 is also in α1 of PTB and is critical for interacting with the Pro residue in the NPxF motif; see Figure 3C and D) with Glu disrupted PTB's binding to the SynGAP NPxF motif (Figure 3L).

## Identification of new AIDA-1 binding partners

The structure of the AIDA-1-PTB/SynGAP-NPxF complex indicated that the residues at the positions −7, −5, −3, −2, −1, and 0 from SynGAP-NPxF are particularly critical for binding to AIDA-1-PTB. We thus used the amino acid sequence pattern of "$L_{-7}x_{-6}F_{-5}x_{-4}N_{-3}P_{-2}x_{-1}[F/Y]_0$" to search for potential AIDA-1-PTB binding proteins. The search of the protein sequence database (prosite.expasy.org) returned the Ras and Rab interactor proteins RIN1, RIN2, and RIN3 containing the "$L_{-7}x_{-6}F_{-5}x_{-4}N_{-3}P_{-2}x_{-1}[F/Y]_0$" pattern (Figure 4A). We went back to our affinity purification data and found that RIN1 was also recovered as an AIDA-1d associated protein (Figure S5A). RIN1 is a Rab5 GEF which promotes the internalization of the epidermal growth factor receptor (EGFR) and remodeling of actin cytoskeletons.[34–36] All members of the RIN family possess a GEF domain (also known as a VPS9 domain), which is responsible for Rab5 activation, a RA domain, a proline-rich region, a SH2 domain, and a NPxF motif (Figure 4A).[36–38] RIN1, which is also highly expressed in mature neurons, particularly in brain regions such as hippocampus, cerebral cortex, and amygdala. RIN1 is localized in neuronal cell bodies and dendrites and is especially enriched in the PSD,[39,40] hinting a possible direct interaction between AIDA-1 and RIN1 in synapses.

We next used ITC-based assays to test the interaction between the RIN1 NPxF-motif and AIDA-1. We found that AIDA-1d-ΔN, AIDA-1c-ΔN, and AIDA-1-PTB all bind to RIN1 NPxF with a high affinity (Kd ∼ 30 nM; Figures 4B and 4C). We further showed that the 11-residue RIN1 NPxF motif with the sequence of

**Figure 3. Detailed Interactions between AIDA-PTB and SynGAP-NPxF.** (A) Detailed interactions between AIDA-1-PTB and SynGAP-NPxF. The sidechains or mainchains of the residues involved in the interactions are drawn in the stick model. Dashed lines highlight the distances between interacted atoms. (B) The detailed interactions of region 1 between AIDA-1-PTB and SynGAP-NPxF. The purple dashed lines highlight the intermolecular hydrogen bonding between AIDA-1-PTB and SynGAP NPxF motif. (C) The interactions in region 2 between AIDA-1-PTB and SynGAP-NPxF. (D) The interactions in region 3 between AIDA-1-PTB and SynGAP-NPxF. (E-H) Interactions between AIDA-1c-ΔN and SynGAP-NPxF mutants measured by ITC. (E) WT; (F) L925A; (G) F927A; (H) F927R. AIDA-1c-ΔN (500 μM) in the syringe was titrated into each SynGAP-NPxF mutant (50 μM) in the cell. (I) Table summarizing the ITC-derived binding affinities of various mutants of SynGAP NPxF motif binding to AIDA-1c-ΔN and SynGAP NPxF motif binding to two mutants of AIDA-1c-PTB. (J-L) Interactions between SynGAP NPxF motif peptides with WT and the AIDA-1c-PTB domain mutations measured by ITC. (J) WT AIDA-1c-PTB; (K) L342E AIDA-1c-PTB; (L) F348E AIDA-1c-PTB. SynGAP-NPxF (500 μM) in the syringe was titrated into each AIDA-1c-PTB mutant (50 μM) in the cell.

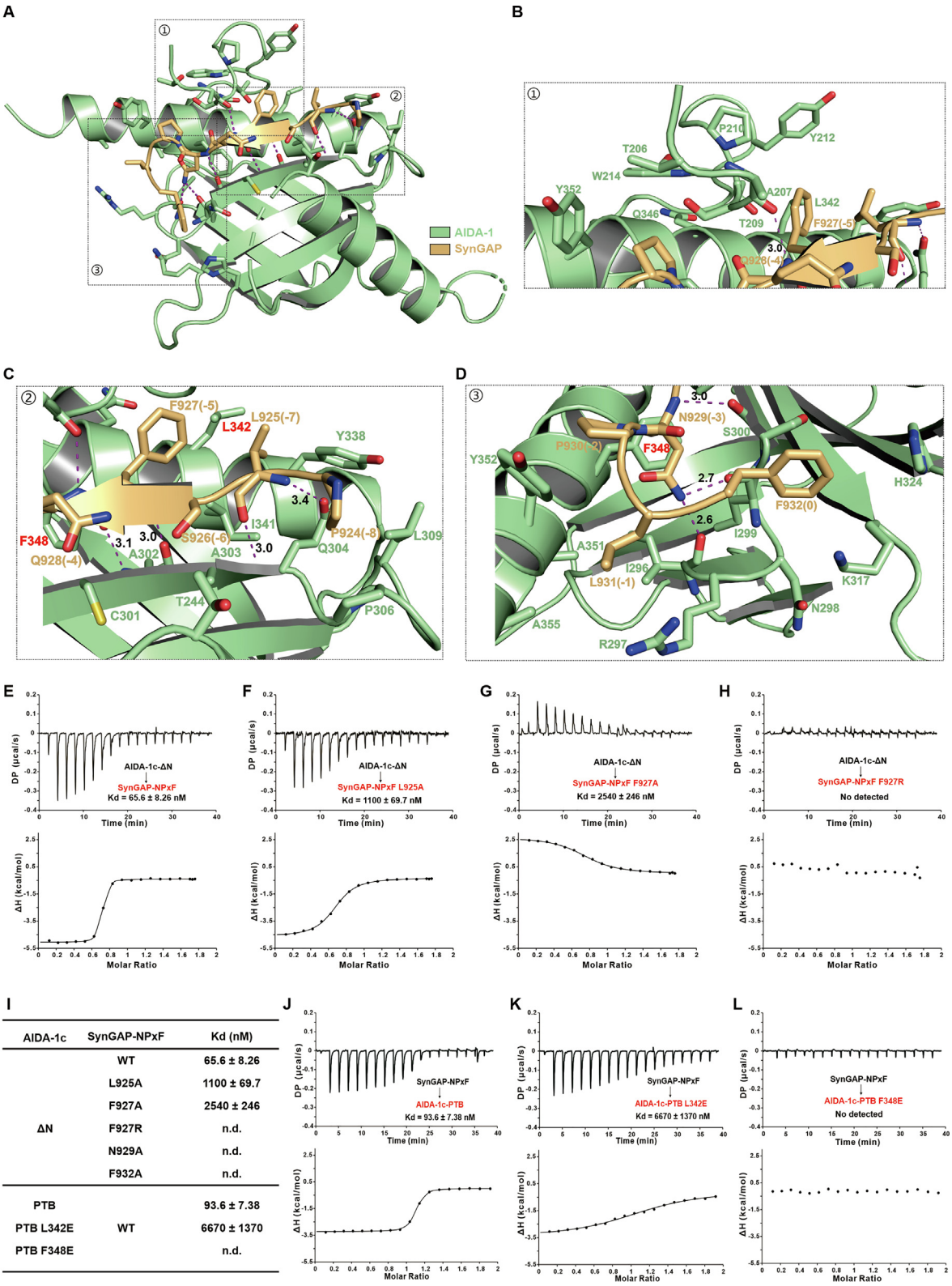


| AIDA-1c | SynGAP-NPxF | Kd (nM) |
|---|---|---|
| ΔN | WT | 65.6 ± 8.26 |
| | L925A | 1100 ± 69.7 |
| | F927A | 2540 ± 246 |
| | F927R | n.d. |
| | N929A | n.d. |
| | F932A | n.d. |
| PTB | | 93.6 ± 7.38 |
| PTB L342E | WT | 6670 ± 1370 |
| PTB F348E | | n.d. |

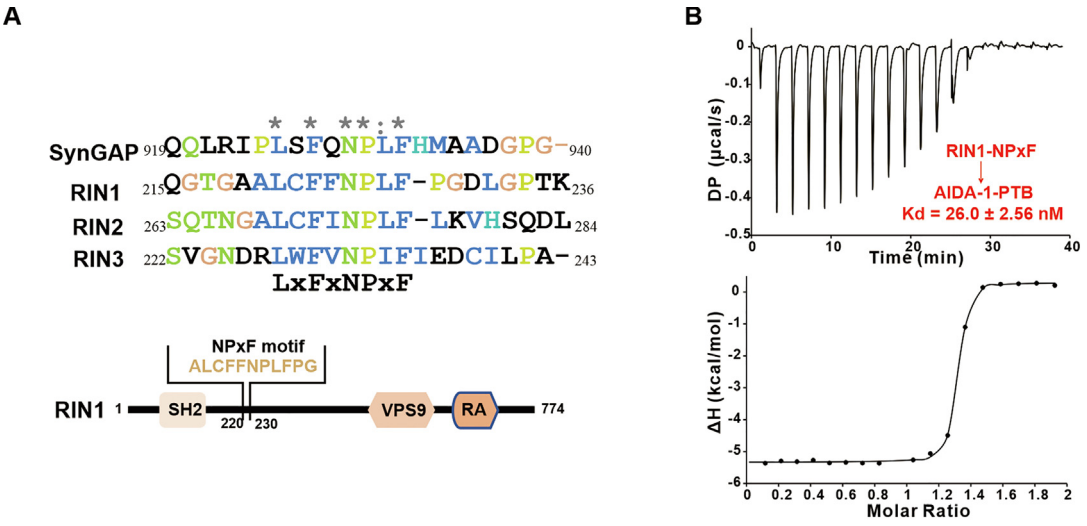


C

| ANKS1B | RIN family | Kd (nM) |
|---|---|---|
| AIDA-1d-ΔN (SAM1SAM2 PTB PBM) | RIN1: ALCFFNPLFPG | 35.9 ± 2.94 |
| AIDA-1c-ΔN (SAM1SAM2 PTB PBM) | RIN1: ALCFFNPLFPG | 26.9 ± 7.47 |
| AIDA-1c-ΔN (SAM1SAM2 PTB PBM) | RIN1: QGTGAALCFFNPLFPGDLGPTK | 32.1 ± 5.69 |
| AIDA-1c 203-360 (203 PTB 360) | RIN1: ALCFFNPLFPG | 26.0 ± 2.56 |
| AIDA-1c-ΔN (SAM1SAM2 PTB PBM) | RIN1: ALCRFNPLFPG | No detected |
| AIDA-1c 203-360 (203 PTB 360) | RIN2: ALCFINPLFLK | 166.0 ± 13.5 |

**Figure 4. The PTB domain of AIDA-1 also binds to the RIN1 NPxF motif.** (A) Schematic diagram showing the domain organization of RIN1 and the alignment of the NPxF motif sequences of SynGAP with those from RIN1/2/3. (B) Interaction between RIN1-NPxF (amino acids 220–230) with AIDA-1-PTB (AIDA-1c aa203–360) measured by ITC. RIN1-NPxF (500 μM) in the syringe was titrated into AIDA-PTB (50 μM) in the cell. (C) Summary of ITC-based measurements of the binding affinities between variant fragments of AIDA-1 with RIN1, and the binding of AIDA-1c-PTB with the 11-residue RIN2 peptide (amino acids 268–278).

"ALCFFNPLFPG" is sufficient for RIN1 to bind to AIDA-1 (Figure 4C). The substitution of the hydrophobic residue Phe(−5) of RIN1 with Arg abolished RIN1's binding to AIDA-1 (Figure 4C). Thus, we conclude that RIN1 can bind strongly to AIDA-1 via the same mechanism as that characterized for the SynGAP/AIDA-1 interaction above.

Finally, we validated that the corresponding 11-residue RIN2 NPxF motif with the sequence of "ALCFINPLFLK" binds to AIDA-1 PTB with a Kd ∼ 166 nM (Figures 4C and S5B). The corresponding 11-residue peptide from RIN3 was insoluble presumably due to its hydrophobicity, and we were not able to measure its binding to AIDA-1.

## Discussion

In this concise study, discovered via affinity purification that AIDA-1 binds to three members of the SynGAP family RasGAPs (SynGAP, Dab2IP and RASAL2) with high affinity and specificity. The PTB domain of AIDA-1 binds to an 11-residue NPx[F/Y]-motif containing peptide fragment in SynGAP family. The structure of the AIDA-1 PTB/SynGAP-NPxF complex, together with detailed biochemical analysis, uncovers a consensus AIDA-1 PTB binding peptide sequence of "$L_{-7}x_{-6}F_{-5}x_{-4}N_{-3}P_{-2}x_{-1}[F/Y]_0$". Compared to the canonical PTB binding targets that are typically either with a core NPx[F/Y] sequence[33,41–43] or a FxNPx[F/Y] sequence,[30,44,45] AIDA-1 PTB recognizes addi-

tional 2–3 residues further upstream the NPx[F/Y] motif. Replacing Leu(−7) with Ala reduced the AIDA-1-PTB/SynGAP-NPxF complex interaction by ~20-fold (Figure 3J), pointing to the critical role of these additional 2–3 residues for the AIDA-1 PTB binding. Using the "$L_{-7}x_{-6}F_{-5}x_{-4}N_{-3}P_{-2}x_{-1}[F/Y]_0$" sequence as the searching pattern, we discovered that the Ras and Rab interactors, RIN1/2/3, may also be specific AIDA-1 binders. RIN1 is known to be expressed in the brain and our affinity purification also recovered RIN1 as a potential AIDA-1 binder. We verified that RIN1 and RIN2 indeed directly bind to AIDA-1 with very strong affinities. The discovery of the strong binding of AIDA-1 to the three SynGAP family RasGAPs and the RIN family Rab GEFs hints that AIDA-1 may act as a hub scaffold in assembling and targeting these small GTPase regulatory enzymes for synaptic functions. Given that small GTPases are critically important for both the development and plasticity of synapses, further research is needed to elucidate the exact roles of AIDA-1 in regulating GTPases activities and consequent synaptic functions. Additionally, the PTB domain of AIDA-1 is extremely similar to that of ANKS1A (Figure S6A). Thus, the structural and biochemical results presented in this work can also guide future studies of the PTB binding targets of ANKS1A.

AIDA-1 was discovered as a protein associated with the cytoplasmic tail of APP.[23,24] However, the interaction between AIDA-1 PTB the NPxY motif of APP is very weak (Kd ~ 10 μM).[23,46] We notice that a short AIDA-1 PTB domain lacking the N-terminal extension as described in this study was used for the reported binding assays.[23,46] We repeated the binding assay using the extended AIDA-1 PTB used in this study and a 12-residue APP NPxY peptide (QNGYENPTYKFF, residues 661–672) by ITC and the derived Kd of the binding is 3.2 ± 0.7 μM (Figure S6B). Given the extremely high abundance of SynGAP (and other specific AIDA-1 binding partners identified in this study), it is unlikely that APP can compete with SynGAP in binding to AIDA-1. Whether APP may interact with AIDA-1 in soma or in axon of neurons remains to be investigated.

The direct and strong interaction between AIDA-1 and SynGAP has multiple implications in synaptic functions. Both proteins are highly abundant in synapses.[1,12,18,47] The structure and biochemical analysis of the AIDA-1-PTB/SynGAP-NPxF indicate that the AIDA-1/SynGAP complex is very stable and not likely to be influenced by posttranslational modifications including phosphorylation. This explains the observations that both SynGAP and AIDA-1 can undergo neuronal activity-dependent co-movement from the PSD core to the PSD pallium,[13,15–17] likely via forming a complex of the two proteins. The AIDA-1/SynGAP complex does not totally disperse from activated synapses, but instead remains at the pallium of PSD, where the lower layer of PSD scaffold proteins such as Shank and Homer are abundantly present. It is possible that the AIDA-1/SynGAP complex (both proteins contain a PBM) may bind to Shank PDZ,[48] and thus maintain the AIDA-1/SynGAP complex with the PSD area for timely responding to next round of synaptic stimulations. The tight association between AIDA-1 and SynGAP also provides a mechanistic explanation for the observed overlaps in the clinical phenotypes of patients with mutations in *SYNGAP1* or in *ANKS1B*. Thus, the results presented in this study will have tremendous implications in understanding the molecular mechanisms of and searching for therapeutic approaches for the brain disorders caused by *SYNGAP1* or in *ANKS1B* mutations.

## Materials and Methods

### Constructs, peptides, protein expression and purification

The corresponding NCBI accession numbers of various proteins used in this study are summarized in Table 2. The full-length and fragments of the *ANKS1B* gene were PCR amplified from a mouse brain cDNA library. Different mutations or shorter fragments of SynGAP, Dab2IP, RASAL2, and RIN1 were generated using the standard PCR-based methods and verified via DNA sequencing. For protein expression, each corresponding coding sequence was cloned into a modified pET32M.3C vector.

Proteins were expressed at 16 °C using *Escherichia coli* BL21 CodonPlus cells, and purification was achieved through a combination of a nickel-NTA agarose affinity chromatography, an ion exchange chromatography, and a size-exclusion chromatography. For all biochemical studies, proteins were purified in a solution composed of 50 mM Tris-HCl pH 8.0, 100 mM NaCl, 1 mM DTT, and 1 mM EDTA. The Trx-$His_6$ tag was cleaved by incubating the recombinant

Table 2 The NCBI accession number of proteins in this study.

| Protein | Reference sequence | Species | Full-length protein |
|---|---|---|---|
| AIDA1b | NP_001121558.2 | Mouse | 1255aa |
| AIDA1c | NP_852063.1 | Mouse | 426aa |
| AIDA1d | NP_001170867.1 | Mouse | 510aa |
| SynGAP | NP_851606.3 | Rat | 1308aa |
| Dab2IP | NP_001107596.1 | Mouse | 1189aa |
| RASAL2 | NP_808312.3 | Mouse | 1286aa |
| RIN1 | NP_001360980.1 | Mouse | 774aa |
| RIN2 | NP_001393437 | Mouse | 903aa |
| RIN3 | NP_808288 | Mouse | 980aa |
| ANKS1A | NP_001272969 | Mouse | 1189aa |
| APP | XP_006522936 | Mouse | 677aa |

protein with HRV 3C protease for 12 h at 4 °C. Subsequently, the tag of each protein was removed through another step of size-exclusion chromatography. The 11-residue SynGAP NPxF peptide (PLSFQNPLFHM) was commercially synthesized.

### Affinity purification coupled with mass spectrometry (AP-MS)

Figure S1A presents the overall process of the AP-MS process. C57BL/6J mice were obtained from Guangdong Medical Laboratory Animal Center, China. Five dissected adult mouse brains were lysed in 10 mL lysis buffer (50 mM Tris-HCl pH 8.0, 300 mM NaCl, 1 mM DTT, and 1 mM EDTA, 0.5% Triton X-100, supplemented with 1 mM PMSF and 1 × halt protease inhibitor cocktail) and centrifuged for 30 min at 40,000*g* at 4. 2 mL cleared extract was first incubated with 20 μL Strep-Tactin Sepharose (IBA Life Sciences) to remove nonspecific beads binding proteins. Then, 1 mL extract was mixed with purified Trx-3 × Strep tag-fused AIDA-1d-ΔN-ΔPBM (amino acids 36–506) or Trx-3 × Strep to a final concentration of 0.5 μM of each bait, respectively. After incubation for 1 h at 4 °C, the mixture was centrifuged for 20 min at 20,000*g* at 4 . Strep-Tactin Sepharose (20 μL) was added to the supernatant and the mixture was incubated for another 30 min with shaking. The beads were then washed three times with PBS and pelleted by centrifugation. Bound proteins were released by boiling the beads with 20 μL SDS-PAGE loading dye for 15 min at 95 °C. SDS-PAGE with Coomassie brilliant blue staining was used to separate and visualize the recovered proteins. Each protein band was sliced from the SDS-PAGE gel and analyzed by liquid chromatography coupled with mass spectrometry (Shanghai Omicsolution Co., Ltd, China).

### Isothermal titration calorimetry (ITC) assay

Isothermal titration calorimetry (ITC) measurements were performed on a MicroCal PEAQ-ITC automated calorimeter (Malvern, UK) at 35 °C. For ITC measurements, proteins were dissolved in an assay buffer composed of 50 mM Tris-HCl pH 8.0, 100 mM NaCl, 1 mM EDTA, and 1 mM DTT. AIDA-1 proteins were each loaded into the syringe in concentrations of 100–500 μM, and NPx[F/Y] motif proteins were loaded into the sample cell of the calorimeter in concentrations of 30–50 μM. The sample from the syringe was injected into the cell at an interval of 120 s, with each injection volume of 2 μL (except that the injection volume for the first titration point was 0.5 μL). The MicroCal PEAQ-ITC Analysis Software was used to analyze the titration data using the one-site binding model.

### Size exclusion chromatography coupled with multi-Angle light scattering (SEC-MALS)

The molar mass of each protein or protein complex was measured using a chromatography system coupled with a multi-angle static light scattering detector (miniDawn, Wyatt) and a differential refractive index detector (Optilab, Wyatt). A Superdex 200 Increase 10/300 GL column (Cytiva) was pre-equilibrated with a buffer of 50 mM Tris-HCl pH 8.0, 100 mM NaCl, 1 mM DTT, and 1 mM EDTA, and then 100 μL of a protein sample typically at 50 μM was loaded to the column. The ASTRA 8 software (Wyatt) was employed to analyze the elution profiles.

### Protein crystallization, data collection and structure determination

Crystals of the AIDA-1b PTB/SynGAP-NPxF complex were grown by sitting drop vapor diffusion at 16 °C in a buffer containing 1.8 M $(NH_4)_2SO_4$, 10% 1,4-Dioxane, and 0.1 M MES at pH 7.1, with protein concentration of 500 μM to 2000 μM in the buffer containing 50 mM Tris-HCl pH 8.0, 100 mM NaCl, 1 mM EDTA, and 1 mM DTT. Crystals were cryoprotected in the crystallization solution with an additional 20% glycerol and flash cooled in liquid nitrogen. Diffraction data were collected at the Shanghai Synchrotron Radiation Facility BL19U1 at 100 K. Data were processed and scaled using HKL3000.[49]

Molecular replacement was used to determine the structure of the complex, with AIDA-1b PTB (PDB: 2M38) as the searching model by PHASER software.[50] Iterative manual adjustments and refinements of the model were carried out using COOT[51] and Refmac.[52] The MolProbity was used to validate the final model and the final statistics were summarized in Table 1. All structure figures were prepared by PyMOL (https://www.pymol.org). The structure reported in this work has been deposited to PDB, with its coordinates and structure factors accessible under the access code of 8YM2.

### CRediT authorship contribution statement

**Xueqian Wang:** Writing – review & editing, Writing – original draft, Investigation, Formal analysis. **Yu Wang:** Writing – review & editing, Writing – original draft, Methodology, Investigation, Formal analysis. **Qixu Cai:** Investigation. **Mingjie Zhang:** Writing – review & editing, Writing – original draft, Supervision, Project administration, Funding acquisition, Conceptualization.

## DECLARATION OF COMPETING INTEREST

The authors declare that they have no known competing financial interests or personal relationships that could have appeared to influence the work reported in this paper.

## Acknowledgements

We thank the BL19U1 beamline at National Facility for Protein Science Shanghai (NFPS) for X-ray beam time. This work was supported by the Ministry of Science and Technology of China (2019YFA0508402), Shenzhen Bay Laboratory (S201101002), Shenzhen Talent Program (KQTD20210811090115021), Shenzhen Science and Technology Basic Research Program (JCYJ20220818100215033), Shenzhen Key Laboratory (ZDSYS20220402111000001), Guangdong Innovative and Entrepreneurial Research Team Program (2021ZT09Y104) to MZ.

## Appendix A. Supplementary data

Supplementary data to this article can be found online at https://doi.org/10.1016/j.jmb.2024.168608.

*Received 8 March 2024;*
*Accepted 8 May 2024;*
*Available online 15 May 2024*

***Keywords***:
AIDA-1;
ANKS1B;
SynGAP;
Dab2IP;
RASAL2

† These authors contributed equally to this work.

## References

1. Carbonell, A.U., Cho, C.H., Tindi, J.O., Counts, P.A., Bates, J.C., Erdjument-Bromage, H., et al., (2019). Haploinsufficiency in the ANKS1B gene encoding AIDA-1 leads to a neurodevelopmental syndrome. *Nature Commun.* **10**
2. Jacob, A.L., Jordan, B.A., Weinberg, R.J., (2010). Organization of amyloid-β protein precursor intracellular domain-associated protein-1 in the rat brain. *J. Comp. Neurol.* **518**, 3221–3236.
3. Kashanchi, F., Hu, V.W., Addington, A., Hyman, A., (2011). Novel autism subtype-dependent genetic variants are revealed by quantitative trait and subphenotype association analyses of published GWAS data. *PLoS One* **6**
4. Uddin, M., Tammimies, K., Pellecchia, G., Alipanahi, B., Hu, P., Wang, Z., et al., (2014). Brain-expressed exons under purifying selection are enriched for de novo mutations in autism spectrum disorder. *Nature Genet.* **46**, 742–747.
5. Chang, X., Lima, L.A., Liu, Y., Li, J., Li, Q., Sleiman, P.M. A., et al., (2018). Common and rare genetic risk factors converge in protein interaction networks underlying schizophrenia. *Front. Genet.* **9**
6. Ren, H., Zhang, C., Huang, C., Li, N., Li, M., Li, Y., et al., (2015). Unravelling genes and pathways implicated in working memory of schizophrenia in Han Chinese. *Int. J. Mol. Sci.* **16**, 2145–2161.
7. Garriock, H.A., Kraft, J.B., Shyn, S.I., Peters, E.J., Yokoyama, J.S., Jenkins, G.D., et al., (2010). A genomewide association study of citalopram response in major depressive disorder. *Biol. Psychiatry* **67**, 133–138.
8. Lydall, G.J., Bass, N.J., McQuillin, A., Lawrence, J., Anjorin, A., Kandaswamy, R., et al., (2011). Confirmation of prior evidence of genetic susceptibility to alcoholism in a genome-wide association study of comorbid alcoholism and bipolar disorder. *Psychiatr. Genet.* **21**, 294–306.
9. Grünblatt, E., Oneda, B., Ekici, A.B., Ball, J., Geissler, J., Uebe, S., et al., (2017). High resolution chromosomal microarray analysis in paediatric obsessive-compulsive disorder. *BMC Med. Genomics* **10**
10. Hashimoto, K., Umehara, H., Numata, S., Tajima, A., Nishi, A., Nakataki, M., et al., (2016). Calcium signaling pathway is associated with the long-term clinical response to selective serotonin reuptake inhibitors (SSRI) and SSRI with antipsychotics in patients with obsessive-compulsive disorder. *PLoS One* **11**
11. Jordan, B.A., Fernholz, B.D., Khatri, L., Ziff, E.B., (2007). Activity-dependent AIDA-1 nuclear signaling regulates nucleolar numbers and protein synthesis in neurons. *Nature Neurosci.* **10**, 427–435.
12. Lowenthal, M.S., Markey, S.P., Dosemeci, A., (2015). Quantitative mass spectrometry measurements reveal stoichiometry of principal postsynaptic density proteins. *J. Proteome Res.* **14**, 2528–2538.
13. Amédée, T., Yang, Y., Tao-Cheng, J.-H., Bayer, K.U., Reese, T.S., Dosemeci, A., (2013). Camkii-mediated phosphorylation regulates distributions of syngap-α1 and -α2 at the postsynaptic density. *PLoS One* **8**
14. Araki, Y., Zeng, M., Zhang, M., Huganir, R.L., (2015). Rapid dispersion of SynGAP from synaptic spines triggers AMPA receptor insertion and spine enlargement during LTP. *Neuron* **85**, 173–189.
15. Dosemeci, A., Toy, D., Burch, A., Bayer, K.U., Tao-Cheng, J.-H., (2016). CaMKII-mediated displacement of AIDA-1 out of the postsynaptic density core. *FEBS Letter* **590**, 2934–2939.
16. Phillips, W.D., Dosemeci, A., Toy, D., Reese, T.S., Tao-Cheng, J.-H., (2015). AIDA-1 moves out of the postsynaptic density core under excitatory conditions. *PLoS One* **10**
17. Yang, Y., Tao-Cheng, J.H., Reese, T.S., Dosemeci, A., (2011). SynGAP moves out of the core of the postsynaptic density upon depolarization. *Neuroscience* **192**, 132–139.
18. Kim, J.H., Liao, D., Lau, L.-F., Huganir, R.L., (1998). SynGAP: a synaptic RasGAP that associates with the PSD-95/SAP90 protein family. *Neuron* **20**, 683–691.
19. Zeng, M., Shang, Y., Araki, Y., Guo, T., Huganir, R.L., Zhang, M., (2016). Phase transition in postsynaptic densities underlies formation of synaptic complexes and synaptic plasticity. *Cell* **166**, 1163–1175.e12.

20. Berryer, M.H., Hamdan, F.F., Klitten, L.L., Møller, R.S., Carmant, L., Schwartzentruber, J., et al., (2013). Mutations inSYNGAP1Cause intellectual disability, autism, and a specific form of epilepsy by inducing haploinsufficiency. *Hum. Mutat.* **34**, 385–394.
21. Gao, Y., Trn, M., Shonai, D., Zhao, J., Soderblom, E.J., Garcia-Moreno, S.A., et al., (2022). Chemico-genetic analysis of native autism proteomes reveals shared biology predictive of functional modifiers. *bioRxiv*. 2022.10.06.511211..
22. Kurabi, A., Brener, S., Mobli, M., Kwan, J.J., Donaldson, L. W., (2009). A nuclear localization signal at the SAM–SAM domain interface of AIDA-1 suggests a requirement for domain uncoupling prior to nuclear import. *J. Mol. Biol.* **392**, 1168–1177.
23. Lakshmana, M.K., Smirnova, E., Shanbhag, R., Kurabi, A., Mobli, M., Kwan, J.J., et al., (2013). Solution structure and peptide binding of the PTB domain from the AIDA1 postsynaptic signaling scaffolding protein. *PLoS One* **8**
24. Ghersi, E., Noviello, C., D'Adamio, L., (2004). Amyloid-β protein precursor (AβPP) intracellular domain-associated protein-1 proteins bind to AβPP and modulate its processing in an isoform-specific manner. *J. Biol. Chem.* **279**, 49105–49112.
25. Fitzgerald, T.W., Gerety, S.S., Jones, W.D., van Kogelenberg, M., King, D.A., McRae, J., et al., (2015). Large-scale discovery of novel genetic causes of developmental disorders. *Nature* **519**, 223–228.
26. Hamdan, F.F., Daoud, H., Piton, A., Gauthier, J., Dobrzeniecka, S., Krebs, M.O., et al., (2011). De novo SYNGAP1 mutations in nonsyndromic intellectual disability and autism. *Biol Psychiatry.* **69**, 898–901.
27. Hamdan, F.F., Gauthier, J., Spiegelman, D., Noreau, A., Yang, Y., Pellerin, S., et al., (2009). Mutations in SYNGAP1 in autosomal nonsyndromic mental retardation. *N. Engl. J. Med.* **360**, 599–605.
28. Parker, M.J., Fryer, A.E., Shears, D.J., Lachlan, K.L., McKee, S.A., Magee, A.C., et al., (2015). De novo, heterozygous, loss-of-function mutations in SYNGAP1 cause a syndromic form of intellectual disability. *Am. J. Med. Genet. A* **167a**, 2231–2237.
29. Stolt, P.C., Jeon, H., Song, H.K., Herz, J., Eck, M.J., Blacklow, S.C., (2003). Origins of peptide selectivity and phosphoinositide binding revealed by structures of disabled-1 PTB domain complexes. *Structure (London, England: 1993)* **11**, 569–579.
30. Uhlik, M.T., Temple, B., Bencharit, S., Kimple, A.J., Siderovski, D.P., Johnson, G.L., (2005). Structural and evolutionary division of phosphotyrosine binding (PTB) domains. *J. Mol. Biol.* **345**, 1–20.
31. Yun, M., Keshvara, L., Park, C.-G., Zhang, Y.-M., Dickerson, J.B., Zheng, J., et al., (2003). Crystal structures of the dab homology domains of mouse disabled 1 and 2*. *J. Biol. Chem.* **278**, 36572–36581.
32. Zhang, Z., Lee, C.-H., Mandiyan, V., Borg, J.-P., Margolis, B., Schlessinger, J., et al., (1997). Sequence-specific recognition of the internalization motif of the Alzheimer's amyloid precursor protein by the X11 PTB domain. *EMBO J.* **16**, 6141–6150.
33. Borg, J.P., Ooi, J., Levy, E., Margolis, B., (1996). The phosphotyrosine interaction domains of X11 and FE65 bind to distinct sites on the YENPTY motif of amyloid precursor protein. *Mol. Cell. Biol.* **16**, 6229–6241.
34. Barbieri, M.A., Kong, C., Chen, P.-I., Horazdovsky, B.F., Stahl, P.D., (2003). The Src homology 2 domain of Rin1 mediates its binding to the epidermal growth factor receptor and regulates receptor endocytosis. *J. Biol. Chem.* **278**, 32027–32036.
35. Hu, H., Bliss, J.M., Wang, Y., Colicelli, J., (2005). RIN1 is an ABL tyrosine kinase activator and a regulator of epithelial-cell adhesion and migration. *Curr. Biol.* **15**, 815–823.
36. Tall, G.G., Barbieri, M.A., Stahl, P.D., Horazdovsky, B.F., (2001). Ras-activated endocytosis is mediated by the Rab5 guanine nucleotide exchange activity of RIN1. *Dev. Cell* **1**, 73–82.
37. Kajiho, H., Saito, K., Tsujita, K., Kontani, K., Araki, Y., Kurosu, H., et al., (2003). RIN3: a novel Rab5 GEF interacting with amphiphysin II involved in the early endocytic pathway. *J. Cell Sci.* **116**, 4159–4168.
38. Saito, K., Murai, J., Kajiho, H., Kontani, K., Kurosu, H., Katada, T., (2002). A novel binding protein composed of homophilic tetramer exhibits unique properties for the small GTPase Rab5. *J. Biol. Chem.* **277**, 3412–3418.
39. Bliss, J.M., Gray, E.E., Dhaka, A., O'Dell, T.J., Colicelli, J., (2009). Fear learning and extinction are linked to neuronal plasticity through Rin1 signaling. *J. Neurosci. Res.*.
40. Deininger, K., Eder, M., Kramer, E.R., Zieglgänsberger, W., Dodt, H.U., Dornmair, K., et al., (2008). The Rab5 guanylate exchange factor Rin1 regulates endocytosis of the EphA4 receptor in mature excitatory neurons. *PNAS* **105**, 12539–12544.
41. Kavanaugh, W.M., Turck, C.W., Williams, L.T., (1995). PTB domain binding to signaling proteins through a sequence motif containing phosphotyrosine. *Science (New York, N.Y.)* **268**, 1177–1179.
42. Zhou, M.M., Ravichandran, K.S., Olejniczak, E.F., Petros, A.M., Meadows, R.P., Sattler, M., et al., (1995). Structure and ligand recognition of the phosphotyrosine binding domain of Shc. *Nature* **378**, 584–592.
43. Zwahlen, C., Li, S.C., Kay, L.E., Pawson, T., Forman-Kay, J.D., (2000). Multiple modes of peptide recognition by the PTB domain of the cell fate determinant Numb. *Embo J.* **19**, 1505–1515.
44. Chen, W.J., Goldstein, J.L., Brown, M.S., (1990). NPXY, a sequence often found in cytoplasmic tails, is required for coated pit-mediated internalization of the low density lipoprotein receptor. *J. Biol. Chem.* **265**, 3116–3123.
45. Eck, M.J., Dhe-Paganon, S., Trüb, T., Nolte, R.T., Shoelson, S.E., (1996). Structure of the IRS-1 PTB domain bound to the juxtamembrane region of the insulin receptor. *Cell* **85**, 695–705.
46. Ghersi, E., Noviello, C., D'Adamio, L., (2004). Amyloid-β protein precursor (AβPP) intracellular domain-associated protein-1 proteins bind to AβPP and modulate its processing in an isoform-specific manner*. *J. Biol. Chem.* **279**, 49105–49112.
47. Cheng, D., Hoogenraad, C.C., Rush, J., Ramm, E., Schlager, M.A., Duong, D.M., et al., (2006). Relative and absolute quantification of postsynaptic density proteome isolated from rat forebrain and cerebellum. *Mol. Cell. Proteom.: MCP.* **5**, 1158–1170.
48. Ali, M., McAuley, M.M., Lüchow, S., Knapp, S., Joerger, A. C., Ivarsson, Y., (2021). Integrated analysis of Shank1 PDZ interactions with C-terminal and internal binding motifs. *Curr. Res. Struct. Biol.* **3**, 41–50.

49. Minor, W., Cymborowski, M., Otwinowski, Z., Chruszcz, M., (2006). HKL-3000: the integration of data reduction and structure solution–from diffraction images to an initial model in minutes. *Acta Crystallogr. D Biol. Crystallogr.* **62**, 859–866.
50. McCoy, A.J., Grosse-Kunstleve, R.W., Adams, P.D., Winn, M.D., Storoni, L.C., Read, R.J., (2007). Phaser crystallographic software. *J. Appl. Cryst.* **40**, 658–674.
51. Emsley, P., Lohkamp, B., Scott, W.G., Cowtan, K., (2010). Features and development of Coot. *Acta Crystallogr. D Biol. Crystallogr.* **66**, 486–501.
52. Murshudov, G.N., Skubák, P., Lebedev, A.A., Pannu, N.S., Steiner, R.A., Nicholls, R.A., et al., (2011). REFMAC5 for the refinement of macromolecular crystal structures. *Acta Crystallogr. D Biol. Crystallogr.* **67**, 355–367.